Non-ellipsometric detection of terahertz radiation using heterodyne EO sampling in the Cherenkov velocity matching scheme

Masahiko Tani,[1,*] Tetsuya Kinoshita,[1] Tomohiro Nagase,[1] Kazuki Horita,[1] Christopher T. Que,[1] Elmer Estacio,[1] Kohji Yamamoto,[1] and Michael I. Bakunov[2]

[1]*Research Center for Development of Far-Infrared Region, University of Fukui, Fukui 910-8507, Japan*
[2]*University of Nizhny Novgorod, Nizhny Novgorod, 603950, Russia*
[*]*tani@fir.u-fukui.ac.jp*

Abstract: A new electro-optic (EO) sampling scheme, which we refer to as "heterodyne EO sampling", for detection of pulsed terahertz (THz) waves is proposed and experimentally demonstrated. In this heterodyne EO sampling scheme, the intensity change in the optical probe pulse induced by a THz field in a nonlinear crystal is measured without any polarization optics. Applied in combination with the non-collinear Cherenkov velocity matching technique, this method allows one to detect pulsed THz waves efficiently and easily using a simpler optical setup as compared to the conventional ellipsometric EO sampling method.

OCIS codes: (190.4223) Nonlinear wave mixing; (040.2235) Far infrared or terahertz.

References and links

1. Q. Wu and X.-C. Zhang, "Free-space electro-optic sampling of terahertz beams," Appl. Phys. Lett. **67**(24), 3523–3525 (1995).
2. D. H. Auston, K. P. Cheung, and P. R. Smith, "Picosecond photoconducting Hertzian dipoles," Appl. Phys. Lett. **45**(3), 284–286 (1984).
3. M. Tani, S. Matsuura, K. Sakai, and S. Nakashima, "Emission characteristics of photoconductive antennas based on low-temperature-grown GaAs and semi-insulating GaAs," Appl. Opt. **36**(30), 7853–7859 (1997).
4. M. Tani, K. Horita, T. Kinoshita, C. T. Que, E. Estacio, K. Yamamoto, and M. I. Bakunov, "Efficient electro-optic sampling detection of terahertz radiation via Cherenkov phase matching," Opt. Express **19**(21), 19901–19906 (2011).
5. P. Y. Han, M. Tani, F. Pan, and X.-C. Zhang, "Use of the organic crystal DAST for terahertz beam applications," Opt. Lett. **25**(9), 675–677 (2000).
6. S. P. Kovalev and G. Kh. Kitaeva, "Two alternative approaches to electro-optical detection of terahertz pulses," JETP Lett. **94**(2), 91–96 (2011).
7. G. Kh. Kitaeva, "Frequency conversion in aperiodic quasi-phase-matched structures," Phys. Rev. A **76**(4), 043841 (2007).
8. G. Kh. Kitaeva, S. P. Kovalev, I. I. Naumova, R. A. Akhmedzhanov, I. E. Ilyakov, B. V. Shishkin, and E. V. Suvorov, "Quasi-phase-matched probe-energy electro-optic sampling as a method of narrowband terahertz detection," Appl. Phys. Lett. **96**(7), 071106 (2010).
9. G. Gallot and D. Grischkowsky, "Electro-optic detection of terahertz radiation," J. Opt. Soc. Am. B **16**(8), 1204–1212 (1999).
10. D. E. Zelmon, D. L. Small, and D. Jundt, "Infrared corrected Sellmeier coefficients for congruently grown lithium niobate and 5 mol.% magnesium oxide-doped lithium niobate," J. Opt. Soc. Am. B. **14**(12), 3319–3322 (1997).
11. L. Pálfalvi, J. Hebling, J. Kuhl, A. Peter, and K. Polgar, "Temperature dependence of the absorption and refraction of Mg-doped congruent and stoichiometric $LiNbO_3$ in the THz range," J. Appl. Phys. **97**(12), 123505 (2005).
12. D. F. Edwards, "Silicon (Si)," in *Handbook of Optical Constant of Solids*, E. D. Palik, ed. (Academic, 1985).
13. C. Winnewisser, P. Jepsen, M. Schall, V. Schyja, and H. Helm, "Electro-optic detection of THz radiation in $LiTaO_3$, $LiNbO_3$ and ZnTe," Appl. Phys. Lett. **70**(23), 3069–3071 (1997).
14. M. Tani, S. Matsuura, K. Sakai, and S. Nakashima, "Emission characteristics of photoconductive antennas based on low-temperature-grown GaAs and semi-insulating GaAs," Appl. Opt. **36**(30), 7853–7859 (1997).
15. T. Nagase, T. Kinoshita, S. Ozawa, K. Kawase, M. I. Bakunov, K. Yamamoto, and M. Tani,"Detection of THz radiation by using optical waveguide structure in Cherenkov-phase-matched EO sampling," in *Proceedings of International Symposium on Frontiers in Terahertz Technology (FTT 2012)*, N. Hiromoto Ed. (Electronically published by FTT 2012 Secretariat, 2012), paper Pos1.26.

#184785 - $15.00 USD Received 4 Feb 2013; revised 22 Mar 2013; accepted 30 Mar 2013; published 8 Apr 2013

1. Introduction

Electro-optic (EO) sampling [1], along with photoconductive sampling [2, 3], is a widely used method for detecting pulsed terahertz (THz) radiation. The efficiency of EO sampling depends on both the EO coefficient of the crystal used for the detection and on the fulfillment of the velocity matching condition between the optical probe pulse and THz waves in the crystal. ZnTe is considered to be the best crystal for THz EO sampling because it has a relatively large EO coefficient (~4 pm/V) and, more importantly, provides perfect velocity matching at the wavelength (near 800 nm) of the mode-locked Ti:sapphire laser, which is the most popular optical source for THz generation and detection. However, the efficiency of EO sampling in ZnTe becomes low at other wavelengths, such as 1.55 μm, where robust and cost-effective femtosecond fiber lasers are available. Recently, an EO sampling scheme based on Cherenkov (non-collinear) velocity matching in a Si-prism-coupled $LiNbO_3$ (LN) crystal was proposed and experimentally demonstrated [4]. In this scheme, the optical probe beam propagates in a LN crystal near its lateral surface whereas THz radiation is input to the crystal through this surface at the Cherenkov angle with use of a Si-prism coupler. For an 800-nm wavelength probe beam, the efficiency of the Cherenkov velocity matched EO sampling scheme was shown to be comparable to that of the conventional collinear EO sampling scheme with ZnTe. More importantly, the Cherenkov scheme can be easily adapted to an arbitrary wavelength of the optical probe beam by proper selection of the apex angle of the coupling Si prism. High THz absorption of LN does not impede the efficiency of the Cherenkov scheme due to a short propagation distance of the THz radiation from the crystal surface to the probe beam. Using a LN crystal for EO sampling is, however, hindered by its strong intrinsic birefringence, which can lead to a spatial separation of the orthogonally polarized components of the optical probe pulse and, therefore, to deterioration of the EO signal. To compensate the phase retardation induced by the intrinsic birefringence, special efforts, such as used in [4, 5], should be made. This inevitably complicates the EO sampling optics.

In this paper, we propose and experimentally demonstrate a new EO sampling scheme, which we refer to as "heterodyne EO sampling," for detection of pulsed THz radiation. In this heterodyne EO sampling scheme, the intensity change in the optical probe pulse induced by a THz field in a nonlinear crystal is measured without any polarization optics. Our heterodyne EO sampling is similar, in principle, to the "energy sensitive EO detection" reported recently by Kovalev and Kitaeva [6] (see also [7, 8]). In [6], however, collinear propagation of the THz and optical probe beams was considered. In this geometry, it was concluded that the energy sensitive EO detection is less efficient than the conventional ellipsometric method: the efficiency is reduced by a factor of Ω/ω_0, where Ω and ω_0 are the THz and optical frequencies, respectively. Unlike [6], we show here that measuring the intensity modulation of the probe pulse can be as efficient as the conventional ellipsometric method, when it is applied in combination with the non-collinear Cherenkov velocity matching technique.

In the following section, we explain the working principle of the heterodyne EO sampling. Then, we experimentally demonstrate the heterodyne EO detection of THz radiation by using Cherenkov velocity matching in a Si-prism-coupled LN crystal. We show that the heterodyne EO signal depends on the lateral position across the optical probe beam. Namely, the heterodyne signals of opposite polarities from the difference-frequency generation (DFG) and sum-frequency generation (SFG) are spatially separated in the probe beam and this makes the heterodyne method efficient. It is also demonstrated that the efficiency can be additionally increased by using wavefront-division balance detection, where the DFG and SFG signals are summed up constructively and the dc background signal is subtracted thus enhancing the signal and suppressing the noise.

2. Principle of heterodyne EO sampling

Figure 1 shows the Cherenkov velocity matching scheme. The probe laser beam is focused by a lens to an entrance facet of a LN slab attached to a Si prism. The laser pulse propagates in

#184785 - $15.00 USD Received 4 Feb 2013; revised 22 Mar 2013; accepted 30 Mar 2013; published 8 Apr 2013

the slab in the + x-direction with the group velocity $V = c/n_g$, where n_g is the optical group refractive index of LN and c is the speed of light. The THz wave is coupled to the LN slab by the Si prism (the THz beam is normal to the prism surface) and propagates synchronously with the probe laser pulse along the x-axis, i.e., $n_g = n_{Si}\sin\alpha$, where n_{Si} is the THz refractive index of Si and α is the apex angle of the prism (the incidence angle of the THz wave on the Si-LN interface) [4]. The c-axis of the LN crystal is assumed to be along the y-axis, as well as the polarizations of the THz wave and the probe optical beam.

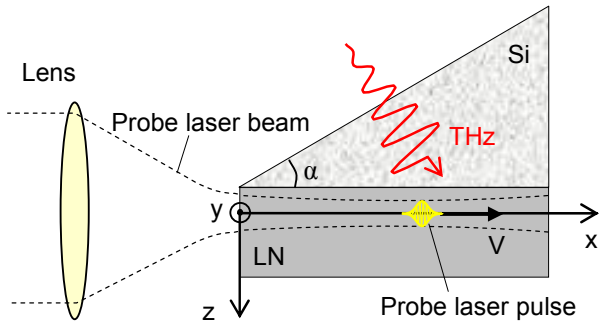

Fig. 1. The Cherenkov velocity matching scheme for heterodyne EO sampling.

We assume that the probe optical beam is wide enough that diffraction effects can be neglected and the beam considered as a quasiplane wave. The electric field of the probe optical pulse at $x = 0$ has the envelope $A_0(t)$, central frequency ω_0, and Fourier spectral amplitude $\tilde{A}_0(\omega)$ (~will denote quantities in the Fourier domain):

$$E_y(0,t) = \mathrm{Re}\left[A_0(t)e^{-i\omega_0 t}\right] = \int_{-\infty}^{+\infty} d\omega \tilde{A}_0(\omega)e^{-i\omega t}. \quad (1)$$

If the optical pulse was propagating in LN without any interaction, its electric field at an arbitrary position x could be expressed as

$$E_y(x,t) = \int_{-\infty}^{\infty} d\omega \tilde{E}_y(x,\omega)e^{-i\omega t}, \quad \tilde{E}_y(x,\omega) = \tilde{A}_0(\omega)e^{ik(\omega)x}, \quad (2)$$

where $k(\omega) = n_{opt}\omega/c$, n_{opt} is the optical refractive index of LN, and c is the speed of light. However, the pulse is modulated in the course of its propagation due to nonlinear interaction with the THz wave.

The THz wave propagates in the LN slab obliquely with respect to the x-axis – under the angle $\cos\beta = (n_{Si}/n_{LN})\sin\alpha$ with n_{LN} the THz refractive index of LN (we neglect dispersion at the THz frequencies). The THz electric field $E_y^{THz}(x,z,t)$ is a given function, which can be presented in a form similar to Eq. (2):

$$E_y^{THz}(x,z,t+\tau) = \int_{-\infty}^{\infty} d\Omega \tilde{E}_y^{THz}(x,z,\tau,\Omega)e^{-i\Omega t} = \int_{-\infty}^{\infty} d\Omega \tilde{A}^{THz}(\Omega)e^{-i\Omega(t+\tau)+iK_x(\Omega)x+iK_z(\Omega)z}, \quad (3)$$

where τ is the time delay of the optical sampling pulse with respect to the THz wave and $K_x(\Omega) = (\Omega/c)n_{LN}\cos\beta = (\Omega/c)n_{Si}\sin\alpha$ and $K_z(\Omega) = (\Omega/c)n_{LN}\sin\beta = (\Omega/c)\left(n_{LN}^2 - n_{Si}^2\sin^2\alpha\right)^{1/2}$ are the x- and z-components of the THz wave vector in LN. The THz field (3) modulates the optical pulse via nonlinear mixing with its frequency components and generation of the second order nonlinear polarization at the optical frequency ω,

$$\tilde{P}_y^{NL}(x,z,\omega) = 2\varepsilon_0\chi_{eff}^{(2)}\int_0^{\infty} d\Omega\left[\tilde{E}_y(x,\omega-\Omega)\tilde{E}_y^{THz}(x,z,\Omega) + \tilde{E}_y(x,\omega+\Omega)\tilde{E}_y^{THz*}(x,z,\Omega)\right], \quad (4)$$

#184785 - $15.00 USD Received 4 Feb 2013; revised 22 Mar 2013; accepted 30 Mar 2013; published 8 Apr 2013

where $\chi^{(2)}_{\text{eff}}$ is the effective nonlinear susceptibility tensor and ε_0 is the permittivity of free space. In Eq. (4), we assume the modulation of the optical pulse to be weak and therefore use undisturbed expression (2) for the pulse Fourier components, i.e., $\tilde{E}_y(x,\omega\pm\Omega)=\tilde{A}_0(\omega\pm\Omega)e^{ik(\omega\pm\Omega)x}$. Such approximation is typical also for the conventional theory of EO detection, where collinear propagation of the THz wave and probe optical pulse is considered [6–9].

The equation for the Fourier transform of the optical electric field $\tilde{E}_y(x,z,\omega)$ follows directly from Maxwell's equations with $\tilde{P}^{\text{NL}}_y(x,z,\omega)$ included as a source:

$$\frac{\partial^2\tilde{E}_y}{\partial x^2}+\frac{\partial^2\tilde{E}_y}{\partial z^2}+k^2(\omega)\tilde{E}_y=-\mu_0\omega^2\tilde{P}^{\text{NL}}_y(x,z,\omega), \tag{5}$$

where μ_0 is the permeability of free space. Applying the Fourier transform with respect to z (with g the corresponding Fourier variable) to Eq. (5) and using an identical equation

$$\frac{1}{2\pi}\int_{-\infty}^{\infty}dz e^{-i(g\mp K_z)z}=\delta\left[g\mp K_z(\Omega)\right]=\frac{1}{K_z'}\delta\left(\Omega-\Omega_g\right), \tag{6}$$

where $K_z'=dK_z/d\Omega=(n_{\text{LN}}/c)\sin\beta$, $\Omega_g=|g|/K_z'$, and δ is the ordinary delta-function, we obtain

$$\begin{aligned}\frac{\partial^2\tilde{E}_y}{\partial x^2}+k_x^2\tilde{E}_y=-\frac{2\omega^2}{c^2K_z'}\chi^{(2)}_{\text{eff}}\Big[&\tilde{A}_0\left(\omega-\Omega_g\right)\tilde{A}^{\text{THz}}(\Omega_g)e^{ik\left(\omega-\Omega_g\right)x+iK_x\left(\Omega_g\right)x-i\Omega_g\tau}\\&+\tilde{A}_0\left(\omega+\Omega_g\right)\tilde{A}^{\text{THz}*}(\Omega_g)e^{ik\left(\omega+\Omega_g\right)x-iK_x\left(\Omega_g\right)x+i\Omega_g\tau}\Big],\end{aligned} \tag{7}$$

where $k_x^2=k^2(\omega)-g^2$ and the first and second terms in the right hand side equal zero for $g<0$ and $g>0$, respectively. We further use the slowly varying envelope approximation and look for a solution of Eq. (7) in the form

$$\tilde{E}_y=\tilde{A}(x,g,\omega)e^{ik_xx}. \tag{8}$$

By substituting Eq. (8) into Eq. (7) we obtain the equation for $\tilde{A}(x,g,\omega)$:

$$\begin{aligned}\frac{\partial\tilde{A}}{\partial x}=\frac{i\omega^2}{c^2k_xK_z'}\chi^{(2)}_{\text{eff}}\Big[&\tilde{A}_0\left(\omega-\Omega_g\right)\tilde{A}^{\text{THz}}(\Omega_g)e^{i(\Delta k)_+x-i\Omega_g\tau}\\&+\tilde{A}_0\left(\omega+\Omega_g\right)\tilde{A}^{\text{THz}*}(\Omega_g)e^{-i(\Delta k)_-x+i\Omega_g\tau}\Big],\end{aligned} \tag{9}$$

where $(\Delta k)_\pm=K_x\left(\Omega_g\right)\pm k\left(\omega\mp\Omega_g\right)\mp k_x$. The integration of Eq. (9) over the interaction interval $0<x<L$, i.e., the intersection length of the THz and optical beams, gives

$$\begin{aligned}\tilde{A}(L,g,\omega)=\tilde{A}_0(\omega)\delta(g)+\frac{i\omega^2L}{c^2k_xK_z'}\chi^{(2)}_{\text{eff}}\Big\{&\tilde{A}_0\left(\omega-\Omega_g\right)\tilde{A}^{\text{THz}}\left(\Omega_g\right)\sin c\left[\frac{(\Delta k)_+L}{2}\right]e^{i(\Delta k)_-L/2-i\Omega_g\tau}\\&+\tilde{A}_0\left(\omega+\Omega_g\right)\tilde{A}^{\text{THz}*}\left(\Omega_g\right)\sin c\left[\frac{(\Delta k)_-L}{2}\right]e^{-i(\Delta k)_-L/2+i\Omega_g\tau}\Big\}.\end{aligned} \tag{10}$$

By applying the inverse Fourier transform with respect to g to Eq. (8) with $\tilde{A}(L,g,\omega)$ given by Eq. (10), we obtain $\tilde{E}_y(x,z,\omega)$ at an arbitrary distance x ($x>L$):

#184785 - $15.00 USD Received 4 Feb 2013; revised 22 Mar 2013; accepted 30 Mar 2013; published 8 Apr 2013

$$\tilde{E}_y(x,z,\omega) = \tilde{A}_0(\omega)\, e^{ik(\omega)x} + \frac{i\omega^2 L}{c^2}\chi^{(2)}_{\text{eff}} \int_0^\infty d\Omega \frac{e^{ik_x x}}{k_x} \left\{ \tilde{A}_0(\omega-\Omega)\, \tilde{A}^{\text{THz}}(\Omega) \sin c\left[\frac{(\Delta k)_+ L}{2}\right] e^{iK_z z + i(\Delta k)_+ L/2 - i\Omega\tau} + \tilde{A}_0(\omega+\Omega)\, \tilde{A}^{\text{THz}*}(\Omega) \sin c\left[\frac{(\Delta k)_- L}{2}\right] e^{-iK_z z - i(\Delta k)_- L/2 + i\Omega\tau} \right\}. \quad (11)$$

In Eq. (11), we changed the integration variable from g to Ω_g and then dropped the subscript g. The first and second terms under the integral in Eq. (11) describe, respectively, the processes of sum frequency generation (SFG) and difference frequency generation (DFG). It is seen from Eq. (11) that the contributions to the optical field at the frequency ω generated via SFG and DFG are proportional to $\exp(-i\omega t + ik_x x \pm iK_z z)$, respectively, and therefore they propagate in slightly different directions. This characteristic feature of the non-collinear wave mixing plays a fundamental role in the heterodyne EO sampling, as will be shown below. A graphical illustration of the non-collinear phase-matching for SFG and DFG processes is given in Fig. 2.

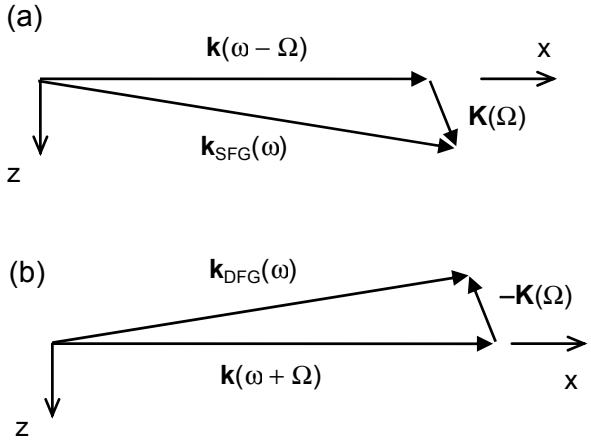

Fig. 2. Wave vector diagrams for non-collinear (a) SFG and (b) DFG processes.

Since Ω << ω, we can neglect the group velocity dispersion and approximate the wavenumber mismatches $(\Delta k)_\pm$ in Eq. (11) as

$$(\Delta k)_\pm \approx K_x(\Omega) - \frac{\Omega}{V} \pm \frac{K_z^2}{2k} = \frac{\Omega}{c}\left(n_{\text{Si}} \sin\alpha - n_g\right) \pm \frac{K_z^2}{2k}. \quad (12)$$

According to Eq. (12) the mismatches for SFG, $(\Delta k)_+$, and DFG, $(\Delta k)_-$, processes are different. For the accurate Cherenkov synchronism $n_g = n_{\text{Si}}\sin\alpha$, for example, $(\Delta k)_\pm = \pm K_z^2/(2k)$. We will also use approximations $1/k_x \approx 1/k$ and $\exp(ik_x x) \approx \exp(ikx)$ in Eq. (11).

By applying the inverse Fourier transform with respect to ω to Eq. (11) we obtain the optical field at an arbitrary distance x ($x > L$):

$$E_y(x,z,t) = \int_{-\infty}^{\infty} d\omega \left[\tilde{A}_0(\omega) + \Delta\tilde{A}(L,z,\omega)\right] e^{-i\omega t + ik(\omega)x}. \quad (13)$$

where $\Delta\tilde{A}$ stands for the second term in the right-hand side of Eq. (11) [without $\exp(ik_x x)$].

The heterodyne EO sampling signal is the change in the integrated optical intensity:

#184785 - $15.00 USD Received 4 Feb 2013; revised 22 Mar 2013; accepted 30 Mar 2013; published 8 Apr 2013

$$\Delta I = \int_{-\infty}^{\infty} dt \left[E_y(x,t) H_z^*(x,t) - E_y(0,t) H_z^*(0,t) \right], \tag{14}$$

where $H_z = n_{\text{opt}}(\varepsilon_0/\mu_0)^{1/2} E_y$ is the magnetic field of the optical pulse. Using an identical equation

$$\int_{-\infty}^{\infty} dt e^{-i(\omega-\omega')t} = 2\pi\delta(\omega-\omega') \tag{15}$$

and Eqs. (11), (13), we present Eq. (14) in the form

$$\begin{aligned} \Delta I = 2\pi\varepsilon_0 L \chi_{\text{eff}}^{(2)} \int_0^{\infty} d\Omega \Bigg\{ & i\tilde{A}^{\text{THz}}(\Omega) \operatorname{sinc}\left[\frac{(\Delta k)_+ L}{2} \right] e^{iK_z z + i(\Delta k)_+ L/2 - i\Omega\tau} \int_{-\infty}^{\infty} d\omega \omega \tilde{A}_0(\omega-\Omega) \tilde{A}_0^*(\omega) \\ & + i\tilde{A}^{\text{THz}*}(\Omega) \operatorname{sinc}\left[\frac{(\Delta k)_- L}{2} \right] e^{-iK_z z - i(\Delta k)_- L/2 + i\Omega\tau} \int_{-\infty}^{\infty} d\omega \omega \tilde{A}_0(\omega+\Omega) \tilde{A}_0^*(\omega) + \text{c.c.} \Bigg\} \end{aligned} \tag{16}$$

with c.c. standing for the complex conjugate. Taking into account that $\Omega << \omega_0$, we put $k(\omega) \approx k(\omega_0) \equiv k_0$ in $(\Delta k)_{\pm}$ and approximate the integrals on ω in Eq. (16) as [9]

$$\int_{-\infty}^{\infty} d\omega \omega \tilde{A}_0(\omega \pm \Omega) \tilde{A}_0^*(\omega) \approx \omega_0 C(\Omega), \tag{17}$$

where $C(\Omega)$ is the autocorrelation function of the optical pulse

$$C(\Omega) = \int_{-\infty}^{\infty} d\omega \tilde{A}_0(\omega \pm \Omega) \tilde{A}_0^*(\omega). \tag{18}$$

Thus, Eq. (16) reduces to

$$\begin{aligned} \Delta I = 2\pi\varepsilon_0 L \omega_0 \chi_{\text{eff}}^{(2)} \int_0^{\infty} d\Omega C(\Omega) \Bigg\{ & i\tilde{A}^{\text{THz}}(\Omega) \operatorname{sinc}\left[\frac{(\Delta k)_+ L}{2} \right] e^{iK_z z + i(\Delta k)_+ L/2 - i\Omega\tau} \\ & + i\tilde{A}^{\text{THz}*}(\Omega) \operatorname{sinc}\left[\frac{(\Delta k)_- L}{2} \right] e^{-iK_z z - i(\Delta k)_- L/2 + i\Omega\tau} + \text{c.c.} \Bigg\}. \end{aligned} \tag{19}$$

It can be seen from Eq. (19) that $\Delta I = 0$, if $(\Delta k)_+ = (\Delta k)_-$. Indeed, in this case the SFG and DFG terms in Eq. (19) (the first and second terms under the integral, respectively, and their c.c.) compensate each other. This case corresponds to the conventional collinear EO sampling geometry ($K_z = 0$). A nonzero EO sampling signal in the collinear geometry can be obtained only if the term of the next order of smallness (~Ω [9]) is included into the approximation (17). This means that in the collinear geometry the heterodyne, or "energy sensitive" [6], detection is less efficient (reduced by a factor of ~Ω/ω_0) as compared to the ellipsometric detection, in accordance with the conclusion of [6].

However, in the non-collinear geometry under consideration the heterodyne EO signal ΔI can be comparable to the ordinary ellipsometric signal for the following reasons. First, according to Eq. (12) the wavenumber mismatches $(\Delta k)_+$ and $(\Delta k)_-$ can differ substantially. The difference in $(\Delta k)_{\pm}$ will lead to a difference in the phase mismatches for SFG and DFG: $(\Delta k)_+ L/2 - (\Delta k)_- L/2 \approx K_z^2 L/(2k_0)$. As a result, the SFG and DFG terms will not compensate each other in Eq. (19). For example, in the case of accurate Cherenkov synchronism $n_g = n_{Si}\sin\alpha$, when $(\Delta k)_{\pm} = \pm K_z^2/(2k_0)$, Eq. (19) reduces to

$$\Delta I = -8\pi\varepsilon_0 L \omega_0 \chi_{\text{eff}}^{(2)} \int_0^{\infty} d\Omega C(\Omega) \operatorname{sinc}\left(\frac{K_z^2 L}{4k_0} \right) \sin\left(\frac{K_z^2 L}{4k_0} \right) \text{Re}\left[\tilde{A}^{\text{THz}}(\Omega) e^{-i\Omega\tau + iK_z z} \right]. \tag{20}$$

#184785 - $15.00 USD Received 4 Feb 2013; revised 22 Mar 2013; accepted 30 Mar 2013; published 8 Apr 2013

For $2\pi c/\omega_0$ = 780 nm, n_{opt} ≈2.2 [10], n_{LN} = 4.75 [11], n_{Si} = 3.418 [12], α = 41° (β ≈62°) [4], and $\Omega/(2\pi)$ = 0.5 THz, $K_z^2 L/(4k_0)$ can be estimated as ~0.027L, where L is taken in mm. Thus, the factor $\sin c\left(\frac{K_z^2 L}{4k_0}\right)\sin\left(\frac{K_z^2 L}{4k_0}\right)$ in Eq. (20) can reach its maximum ≈0.72 at L ~43 mm, and the heterodyne signal (20) becomes of the same order of magnitude as the ellipsometric one, cf [8]. For other frequencies, the corresponding length L can be estimated using the relation $K_z^2 L/(4k_0) \propto \Omega^2$.

Second, even more essentially, the SFG and DFG contributions to ΔI are separated spatially. Although this does not explicitly follow from Eq. (19) due to our approximation of infinitely wide optical and THz beams, the effect of separation was already illustrated on the basis of Eq. (11) and Fig. 2. Furthermore, we will confirm this effect experimentally below. Assuming total separation of the SFG and DFG beams we can consider independently the contributions to Eq. (19) from the SFG and DFG processes,

$$\Delta I_{SFG} = -4\pi\varepsilon_0 L\omega_0\chi_{eff}^{(2)}\int_0^\infty d\Omega C(\Omega)\sin c\left[\frac{(\Delta k)_+ L}{2}\right]\mathrm{Im}\left[\tilde{A}^{THz}(\Omega)e^{-i\Omega\tau+i(\Delta k)_+ L/2+iK_z z}\right], \quad (21)$$

$$\Delta I_{DFG} = -4\pi\varepsilon_0 L\omega_0\chi_{eff}^{(2)}\int_0^\infty d\Omega C(\Omega)\sin c\left[\frac{(\Delta k)_- L}{2}\right]\mathrm{Im}\left[\tilde{A}^{THz*}(\Omega)e^{i\Omega\tau-i(\Delta k)_- L/2-iK_z z}\right]. \quad (22)$$

By assuming that the spectral distribution of the optical probe pulse is much wider than that of the THz wave (i.e., the optical pulse duration is much shorter than the period of the THz wave), we can approximate $C(\Omega)$ as $C(\Omega) \approx C(0)$, where $C(0) = I_0(\mu_0/\varepsilon_0)^{1/2}(2\pi n_{opt})^{-1}$ and I_0 is the integrated optical intensity at x = 0. By using this approximation and assuming additionally the accurate Cherenkov synchronism, i.e., $n_g = n_{Si}\sin\alpha$, we can present the heterodyne EO sampling signals in the form

$$\frac{\Delta I_{SFG}}{I_0} \approx -\frac{2L\omega_0}{cn_{opt}}\chi_{eff}^{(2)}\int_0^\infty d\Omega \sin c\left(\frac{K_z^2 L}{4k_0}\right)\mathrm{Im}\left[\tilde{A}^{THz}(\Omega)e^{-i\Omega\tau+iK_z^2 L/(4k_0)+iK_z z}\right], \quad (23)$$

$$\frac{\Delta I_{SFG}}{I_0} \approx \frac{2L\omega_0}{cn_{opt}}\chi_{eff}^{(2)}\int_0^\infty d\Omega \sin c\left(\frac{K_z^2 L}{4k_0}\right)\mathrm{Im}\left[\tilde{A}^{THz}(\Omega)e^{-i\Omega\tau-iK_z^2 L/(4k_0)+iK_z z}\right]. \quad (24)$$

By assuming further that $K_z^2 L/(4k_0) << \pi/2$ and taking into account that for the used geometry $\chi_{eff}^{(2)} = r_{33}n_e^4/2$, where n_e is the optical refractive index of the extraordinary wave ($n_e = n_{opt}$, in our previous notation) and r_{33} is the component of the EO tensor, Eqs. (23) and (24) can be simplified to

$$\frac{\Delta I_{SFG}}{I_0} \approx -\frac{\Delta I_{DFG}}{I_0} \approx -\frac{\omega_0 L n_e^3 r_{33}}{c}\int_0^\infty d\Omega\,\mathrm{Im}\left[\tilde{A}^{THz}(\Omega)e^{-i\Omega\tau+iK_z z}\right]. \quad (25)$$

By representing $\tilde{A}^{THz}(\Omega)$ in the form $\tilde{A}^{THz}(\Omega) = \left|\tilde{A}^{THz}(\Omega)\right|\exp\left[i\varphi(\Omega)\right]$, Eq. (25) becomes

$$\frac{\Delta I_{SFG}}{I_0} \approx -\frac{\Delta I_{DFG}}{I_0} \approx \frac{\omega_0 L n_e^3 r_{33}}{c}\int_0^\infty d\Omega\left|\tilde{A}^{THz}(\Omega)\right|\sin\left[\Omega\tau - K_z z - \varphi(\Omega)\right]. \quad (26)$$

At the same time, it follows from Eq. (3) that

$$E_y^{THz}(0,z,\tau) = 2\int_0^\infty d\Omega\left|\tilde{A}^{THz}(\Omega)\right|\cos\left[\Omega\tau - K_z z - \varphi(\Omega)\right]. \quad (27)$$

#184785 - $15.00 USD Received 4 Feb 2013; revised 22 Mar 2013; accepted 30 Mar 2013; published 8 Apr 2013

By comparing Eqs. (26) and (27) one can conclude that the heterodyne EO sampling signal does not represent directly the THz waveform. The amplitude spectrum of the signal is the same as that of the THz waveform; however, all the spectral components are phase delayed by π/2. Thus, the heterodyne EO signal represents the Hilbert transform of $E_y^{\mathrm{THz}}(0,z,\tau)$:

$$\frac{\Delta I_{\mathrm{SFG}}}{I_0} \approx -\frac{\Delta I_{\mathrm{DFG}}}{I_0} \approx \frac{\omega_0 L n_e^3 r_{33}}{2c} \mathrm{H}\left[E_y^{\mathrm{THz}}(0,z,\tau)\right]. \tag{28}$$

The corresponding formula for the ellipsometric EO sampling with a LN crystal is [13]

$$\frac{\Delta I}{I_0} \approx \frac{\left(n_e^3 r_{33} - n_o^3 r_{13}\right)\omega_0 L}{2c} E_y^{\mathrm{THz}}(\tau), \tag{29}$$

where n_o is the optical refractive index of the ordinary wave and r_{33} is another component of the EO tensor. As one can see from comparing Eq. (28) with Eq. (29), the heterodyne and ellipsometric signals are of the same order of magnitude. The heterodyne signal is even somewhat larger due to the subtraction of $n_o^3 r_{13}$ in the numerator of Eq. (29), $n_o^3 r_{13} \approx 0.35 n_e^3 r_{33}$. Note also that realization of the ellipsometric EO sampling scheme with a LN crystal requires additional optics, such as used in [4, 5], to compensate for the phase retardation induced by the intrinsic birefringence of the crystal.

3. Experimental

Figure 3 shows the experimental setup for the heterodyne EO sampling. We used a mode-locked femtosecond fiber laser as an optical source (IMRA America Inc., model C-20-SP). The repetition rate of the laser is 50 MHz and the pulse width of the fundamental oscillations at 1.55 μm is about 200 fs and that of the SHG at 780 nm is about 100 fs. The laser pulses were split into pump and probe beams. The pump beam of 780 nm wavelength and 6 mW average power triggered a photoconductive bow-tie antenna on a low-temperature-grown GaAs substrate, which was biased with a 100 V peak-to-peak, 95-kHz AC voltage. A hyper-hemispherical Si lens having a 13 mm diameter was used as an output coupler for generated THz radiation from the substrate to free space. The THz beam was collimated and focused onto a LN crystal through a right triangular high-resistivity-Si prism by a pair of parabolic mirrors (50 mm diameter and 76 mm focal length). The prism apex angle α (Fig. 1) was 41°, which is complementary to the Cherenkov angle 49° [4], and the incident THz beam was aligned to be normal to the prism slanted face. The 1% MgO-doped stoichiometric LN crystal, bonded to the prism bottom surface, was 2 mm-thick and had 10 × 5 mm^2 lateral dimensions (exactly the same as that of the prism bottom surface). The *c*-axis of the LN crystal was oriented perpendicularly to the triangular face of the prism, and the polarization of the THz radiation was aligned parallel to the *c*-axis. The probe beam of 780 nm or 1.55 μm wavelength (~1 mW average power on the photodetector) was focused onto the 10 × 2 mm^2 facet of the LN crystal by a 200 mm-focus lens. The polarization of the probe beam was parallel to the *c*-axis of the LN crystal. The minimum diameter of the probe beam in the LN crystal is estimated to be about 200 μm. The probe beam intensity modulation by the heterodyne process described in the previous section was detected by a single photodetector with its output signal fed to a lock-in amplifier, using the synchronized output from the AC bias voltage of the THz emitter as the reference signal. A Si PIN and an InGaAs PIN photodiodes were used as a photodetector for the 780 nm and 1.55 μm probe beams, respectively. Note that although we use LN as an EO crystal, there is no need of the complex optical configuration to compensate the parasitic phase retardation caused by birefringence of the LN crystal [4, 5]. This is because in the heterodyne EO sampling method we detect the intensity change of the probe beam, not the polarization change induced by the phase retardation in the beam.

#184785 - $15.00 USD Received 4 Feb 2013; revised 22 Mar 2013; accepted 30 Mar 2013; published 8 Apr 2013

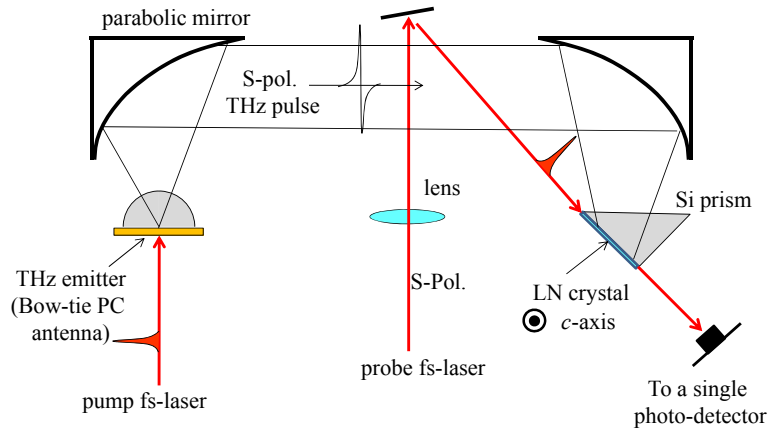

Fig. 3. Schematic of the experimental setup.

4. Results and discussion

Figure 4(a) shows the THz waveforms measured with the Cherenkov-phase-matched LN crystal (LN/Si-prism structure) in the heterodyne EO sampling scheme and, for a comparison, in the ordinary ellipsometric EO sampling scheme reported in [4]. The probe beam wavelength was either 780 nm (the SHG output from the fiber laser) or 1.55 μm (the fundamental) in the heterodyne scheme and 780 nm in the ellipsometric scheme. It is remarkable that the heterodyne and ellipsometric signals are comparable in magnitude, in accordance with our theory in Sec. 2 and contrary to the theoretical and experimental results in [6, 8]. The heterodyne signal obtained with a 1.55 μm wavelength probe beam is about a half of that obtained with a 780 nm beam. This is reasonable because the EO signal is inversely proportional to the optical wavelength, as indicated by Eq. (28). There is a difference in shape between the waveforms obtained with the heterodyne and ellipsometric techniques [Fig. 4(a)]. The difference can be attributed to the fact that the heterodyne signal represents the Hilbert transform of the THz waveform rather than the original waveform, see Eq. (28). In addition, when $K_z^2 L/(4k_0)$ is not negligible, it can influence the shape of the heterodyne signal through the factor $\mathrm{sinc}\left[K_z^2 L/(4k_0)\right]$ and phase factors in Eq. (23) and (24).

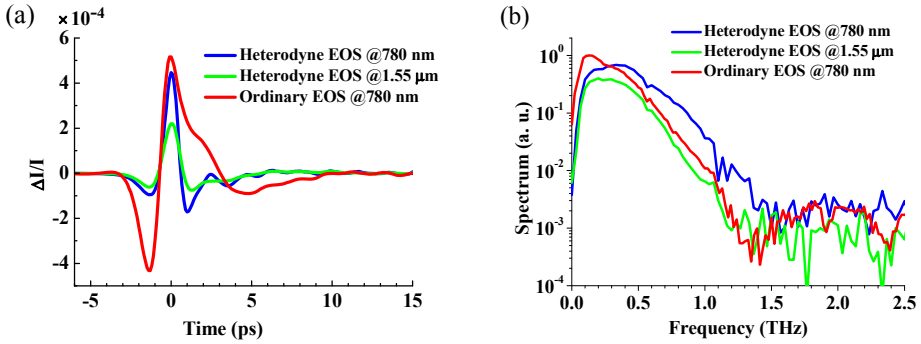

Fig. 4. (a) THz waveforms measured with the LN/Si-prism structure in the heterodyne and ellipsometric schemes. (b) Corresponding Fourier transformed amplitude spectra

Figure 4(b) shows Fourier transformed amplitude spectra of the THz waveforms in Fig. 4(a). All spectra extend to about 1.5 THz. The spectral bandwidth is limited by the properties of the photoconductive bowtie antenna used as an emitter.

#184785 - $15.00 USD Received 4 Feb 2013; revised 22 Mar 2013; accepted 30 Mar 2013; published 8 Apr 2013

The remarkably large heterodyne EO sampling signal observed in our experiment [Fig. 4(a)] can be explained by the mechanism of spatial separation of the SFG and DFG contributions to the probe beam described in Sec. 2. In this mechanism, the optical fields generated via SFG and DFG propagate in slightly different directions, namely, under the angles $\approx(\pm K_z/k)$ to the x-axis [see Eq. (11) and Fig. 2], and in the course of propagation the SFG and DFG beams become non-overlapping. Since the SFG and DFG contributions to the optical intensity are of opposite signs [see, for example, Eq. (25)], they almost compensate for each other when the beams are overlapping. However, the compensation is absent for non-overlapping beams. Importantly, the spatial separation of the SFG and DFG beams is inherent in the non-collinear Cherenkov velocity matching scheme we used for the heterodyne EO sampling, contrary to the conventional collinear geometry considered in [6–9].

In order to verify the proposed mechanism of SFG/DFG spatial separation, we conducted the following experiment. We expanded the 1.55 μm wavelength probe beam, after its passing through the LN crystal, by a lens to a diameter of about 8 mm (FWHM) and measured the intensity change at different positions across the beam by an InGaAs photodiode (Hamamatsu Photonics K.K. InGaAs photodiode G8371-03). To increase the spatial resolution of the measurement, we reduced the active area of the photodiode (about 3 mm) by putting an iris on it. The position of the photodiode was changed by 1 mm steps from $\Delta = -3$ mm to + 9 mm, with $\Delta = 0$ at the center of the probe beam, and THz waveform was measured at each position of the photodiode. Unfortunately, we could not measure the signal at $\Delta < -3$ mm because of the limited length of the translation stage used for the photodiode. The results of the spatially resolved heterodyne EO sampling measurement are shown in Fig. 5. One can see from Fig. 5 that the THz waveform changes continuously with the lateral displacement Δ and the polarity flips near the probe beam center ($\Delta = 0$). The intensity modulation ratio $\Delta I/I$ becomes larger at the positions farther from the probe beam center. The results obtained confirm the proposed mechanism of SFG/DFG spatial separation. Indeed, the signals at $\Delta > 0$ and $\Delta < 0$ can, evidently, be attributed to those from the partially separated SFG and DFG beams. Near the center, where the beams overlap, the signal is smaller.

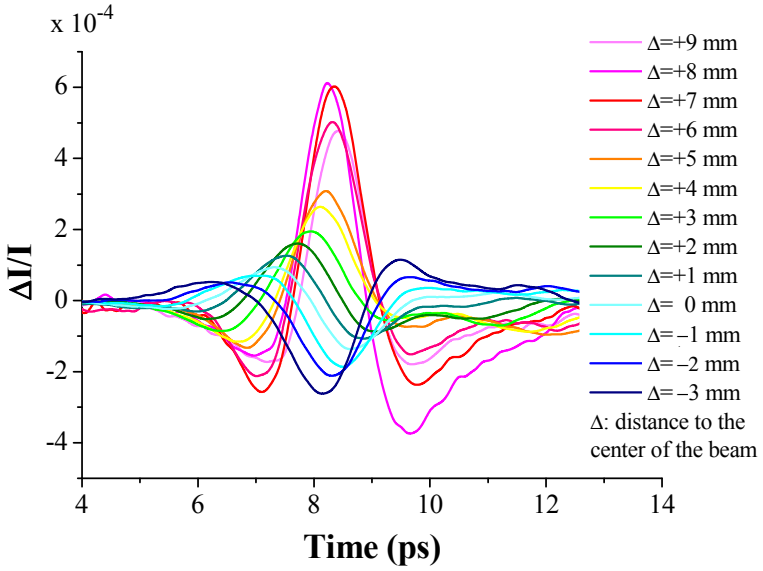

Fig. 5. The heterodyne EO sampling signal for different positions Δ of the photo-detector across the expanded probe beam (Δ is measured from the center of the beam).

By relying on the fact that the polarity of the heterodyne signal flips across the probe beam, we propose further an improvement of the heterodyne EO sampling scheme, such as

#184785 - $15.00 USD Received 4 Feb 2013; revised 22 Mar 2013; accepted 30 Mar 2013; published 8 Apr 2013

the balanced heterodyne detection. The idea of the improvement is to divide the probe beam into two parts, which correspond to the SFG and DFG processes, and make use of the balanced detection by subtracting the SFG and DFG signals received separately by two detectors (photodiodes). Due to opposite polarities of the SFG and DFG signals they are added constructively whereas the background signals from the two photodetectors are subtracted thus improving the signal-to-noise ratio. Contrary to the ordinary ellipsometric EO sampling, where the balanced detection scheme is also used, the probe beam is split by an edged mirror rather than a polarizing beam splitter (a Wollaston prism or polarizing prism cube).

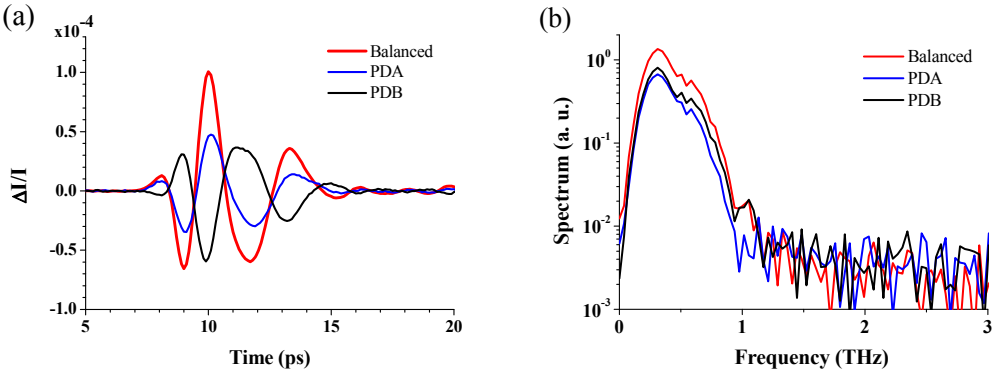

Fig. 6. (a) THz waveforms detected by the balanced (red line) and single-beam (blue and black lines) heterodyne EO sampling. (b) Corresponding Fourier transformed amplitude spectra

The following experiment was carried out to verify the proposed balanced heterodyne detection method. We slightly expanded the probe beam after its passing through the LN/Si-prism structure and divided it into two beams by using an edged mirror. The two separated beams were detected by a pair of balanced photodiodes, PDA and PDB. In this measurement, the 1.55 μm wavelength fundamental output from the fiber laser was used as the probe beam. The THz waveforms obtained by the measurement are shown in Fig. 6(a) and their Fourier transformed amplitude spectra are shown in Fig. 6(b). The THz waveforms detected by a single photodiode, PDA or PDB, were measured by blocking the beam coming to the other photodiode. The THz waveform detected by the balanced heterodyne EO sampling scheme is twice as large in magnitude as that for the single beam detection. It coincides precisely with the result of the summation of the two waveforms detected with PDA and PDB photodiodes (with flipped polarity of one of the waveforms). The noise level estimated from the amplitude spectrum in the frequency range 1.5–5 THz for the balanced detection scheme is reduced by 37% as compared to the single beam detection with PDA or PDB. As a result, the dynamic range defined by the spectral peak amplitude and the noise level was improved by a factor of 3 in the balanced detection scheme. Note that the lower signal level in Fig. 6(a) as compared to Figs. 4(a) and 5 is due to the fact that in this experiment a spiral photoconductive antenna with a 20 Vp-p bias was used rather than a bow-tie antenna with a 100 Vp-p bias as shown in Fig. 3.

The spectral bandwidth of the detected THz signal above the noise level is about 1 THz in Fig. 6(b) and about 1.4 THz and 1.2 THz for the 780 nm and 1.55 μm probe beams, respectively, in Fig. 4(b). In our experiments, the bandwidth was limited mainly by the emission spectrum of the photoconductive antenna used as a THz emitter. For example, the bow-tie antenna has maximum emission efficiency below 0.2 THz [14]. In principle, the main physical factor that limits the potential bandwidth of the heterodyne EO sampling technique is the lateral dephasing of the THz wave over the probe beam diameter as discussed in [4]. Enclosing the probe beam in a thin slab waveguide can circumvent this factor. By using a Si-prism coupled 40 μm thick LN slab, we recently demonstrated a detection bandwidth of about

#184785 - $15.00 USD Received 4 Feb 2013; revised 22 Mar 2013; accepted 30 Mar 2013; published 8 Apr 2013

3 THz for the heterodyne EO sampling technique [15]. Reducing the thickness of the LN slab can further increase the detection bandwidth.

5. Conclusion

To conclude, we have demonstrated "heterodyne EO sampling" of broadband THz radiation in the Cherenkov phase matching scheme with a Si-prism-coupled LN crystal. In this new EO sampling scheme, no polarization optics is required. Therefore, the EO sampling optics is much simplified as compared to the conventional ellipsometric EO sampling, where a set of polarization optics, such as wave-plates, polarizing beam splitter, etc., is required. To increase the heterodyne EO sampling efficiency by a factor of two and to suppress the background noise, the balance detection by wavefront-division of the probe beam has been proposed.

Acknowledgments

Careful reading of the manuscript by Drs. S. Funkner and G. Neihues is gratefully acknowledged. M. I. Bakunov acknowledges support from the Ministry of Education and Science of the Russian Federation through Agreement Nos. 11.G34.31.0011 and 14.B37.21.0770 and from RFBR through grant No. 13-02-92106. M. Tani acknowledges support from Japan Science and Technology Agency (JST) through grant No. AS242Z00696J in "Adaptable and Seamless Technology transfer (A-STEP) Program."